Status of Heating and Current Drive Systems Planned for ITER

M. J. Singh, Heating and Current Drive Teams at ITER Organization, European Domestic Agency, Japan Domestic Agency, Indian Domestic Agency, Russian Federation Domestic Agency, and United States Domestic Agency

***Abstract*— An auxiliary heating power of >70 MW is envisaged at ITER in order to obtain the plasma temperatures and plasma profiles required to achieve $Q > 10$ for 400 s (inductive ELMy H-mode) and $Q = 5$ for a pulse duration of 3600 s (noninductive discharge), for which a potential upgrade may be necessary. In addition to providing the desired heating, the systems are also expected to drive current, tailor the plasma profile, and control the plasma instabilities. It is difficult to realize such a broad range of functionalities through a single system. As a result, three systems are planned during the first operational phase of ITER, which include the neutral beam (NB), electron cyclotron (EC), and ion cyclotron (IC) systems. While the NB systems are expected to deliver 33 MW of heating power to the plasma and drive current through it by the use of two NB injectors, the IC and the EC systems deliver 20 MW each. IC covers a wide variety of heating and current drive schemes and EC heats the electrons providing local heating and current drive, which can be steered across the plasma cross section. These systems, operating in a hostile radiative environment, become radioactive due to the neutron flux from ITER. Coupled to this are the features of long operating pulse lengths at high powers, reduced maintainability, and increased remote handling requirements. As a result, these devices are challenging to realize compared with their present operational counterparts worldwide. In order to help mitigate the risks involved with the manufacturing, setting up, and operation of these systems at ITER, extensive prototyping and research and development (R&D) activities are underway at various laboratories of the participating domestic agencies (DAs) for each of these systems. This paper provides a brief description of the requirements of each of the three heating systems for the various plasma scenarios foreseen for ITER operation, their functional and technical advantages, the various developments over the period of time, and the present status of the prototype and R&D activities underway to realize these systems and the overall development schedule.**

I. Introduction

OVER the years, a mixture of auxiliary heating systems has been used to overcome the limitations of ohmic heating of plasma caused by a decrease in resistivity with an increase in the electron temperature. At ITER [1] four heating systems are envisaged, although lower hybrid (LH) will only be installed if it is chosen as part of the heating systems upgrade. Three of the systems use electromagnetic waves in three frequency ranges, viz., the electron cyclotron (EC), the ion cyclotron (IC), and the LH resonance frequency and the fourth uses multiampere high-energy neutral beams (NBs) [2]. These systems, either individually or in tandem, are designed to cover a range of operational requirements that include delivery of sufficient heating power to the core to access the H-mode confinement regime, and control of the plasma temperature with increasing density to bring the plasma to the desired operating point and to control any deviation around the operating point. In addition, they are foreseen to provide the noninductive central current drive and an off-axis current drive capability for the current profile control. Table I gives a summary of the requirements from each of the four heating devices during the various phases of ITER.

TABLE I

Present and Potential Upgrade Parameters of the ITER HCD Systems

System	Injected power (MW)			Function
	1st Plasma	H-He /D-D /D-T	Potential after upgrade*	
NB	0	33	50	Heating, current drive, current profile tailoring, plasma rotation
IC	0	20	40	Heating, Impurity control, MHD control
EC	6.7	20	40	Current drive, current profile tailoring, MHD control, impurity control
LH	0	0	40	Off axis current drive

*The planned heating system upgrade is from the initial 73 MW to 133 MW, hence not all the potential heating system upgrades will be realised.

The capability of each of the four systems for the various intended uses has been demonstrated on Tokamaks worldwide. However, there are some areas in which each of the four systems need development, from the setting up, commissioning, and operational point of view, and because these systems face a hostile radiative environment at ITER for longer pulse lengths with reduced maintenance and increased remote handling requirements. The risks related to these requirements are being mitigated by extensive research and development (R&D) and prototyping activities on all the systems, wherever it is required, in the various test facilities of the participating domestic agencies (DAs), European domestic agency (EUDA), Japanese domestic agency (JADA), Indian domestic agency (INDA), United States domestic

agency (USDA), and Russian domestic agency (RFDA). This paper provides a brief overview of the requirements, development efforts, and the present status of the EC, IC, and NB systems planned for ITER.

II. EC System

A. Functionality

The EC system at ITER [3], [4] is a unique pinpoint heating and current drive source that is controlled from external actuators far from the plasma. The ability to control the deposited power in a relatively narrow location at the resonance is unique. The deposition width is typically between 2% and 20% of the normalized plasma cross section.

ITER has two EC launching systems; a launcher at the equatorial port (EL), which accesses the plasma core (on axis to midradius), and the other consists of four launchers in upper ports (UL) to access the outer half of the plasma. The design of each of the launchers, access range, power handling, beam focusing, etc., is tailored to their allocated heating and current drive (H&CD) application.

As shown in Table I, the EC H&CD has an application in all the phases of ITER. For each phase, the applications are grouped according to the four periods of the plasma discharge, i.e., plasma initiation, ramp up, flat top, and ramp down [4]. The flat top has been considered as the design driver in determining the steering range and the toroidal injection angles of all the launchers. The ramp up and the ramp down periods require different functionalities from the EC system and will have to adjust to the limitations of the steering range and injected power defined by the present EC system design.

For the convenience of the reader, a brief summary of the functional description of the EC system for all the four periods of the plasma discharge is presented here. Each plasma discharge at ITER will use the EC system for plasma initiation (breakdown and burnthrough). For the breakdown part, up to 6.7 MW of power will be injected using 8, 170 GHz gyrotrons for pulse lengths $\leq$1 s and over a range from half (2.65 T) to full field (5.3 T) with either the first or second harmonic resonance layer inside the torus cross section. During the burnthrough phase, 8 gyrotrons will inject 6.7 MW of power for pulse lengths $\leq$5 s to ensure that the plasma does not collapse due to a high level of radiated power relative to the ohmic power. The need for reflection off the central column places a toroidal limitation of $<25^\circ$ for the beams from the launchers located at the upper and the equatorial ports. Angles greater than 25° are to be avoided for this phase to avoid damage to the diagnostic instrumentation from the stray power entering the diagnostic port plugs. In the plasma current ramp-up phase, the EC will be used to provide central heating and bulk current drive ($\rho_{\text{dep}} \leq 0.5$), current profile tailoring from coelectron to counter electron cyclotron current drive (ECCD) ($\rho_{\text{dep}} \leq 0.3$), off-axis co-ECCD ($0.4 \leq \rho_{\text{dep}} \leq 0.5$), control of sawteeth ($0.4 \leq \rho_{\text{dep}} \leq 0.8$), and to provide neoclassical tearing mode (NTM) control ($0.6 \leq \rho_{\text{dep}} \leq 0.9$) where ρ_{dep} corresponds to the EC deposition location in normalized radius. The L–H mode transition requires sufficient power to be deposited within the pedestal to exceed the desired power threshold. Once the H-mode is formed, EC will continue to provide central heating as well as control of magneto-hydrodynamic (MHD) instabilities. The flat top is the most demanding phase, where multiple events force the allocation of 20 MW of available EC power to various H&CD applications. For the central heating, the power launched from the EL is deposited inside the midradius ($\rho_{\text{dep}} \leq 0.5$). The power is distributed between 67% co-ECCD and 33% counter-ECCD, which provides flexible current profile tailoring. In addition, it decouples heating from the current drive to avoid peaking of the plasma current profile. The full 20 MW can be launched for co-ECCD using the remaining 33% of the 100% from the upper launcher. Typical current drive efficiencies range from 30 kA/MW (15 MA scenario) to 50 kA/MW (9 MA scenario).

In addition to providing heating and current drive, the EC system, because of its unique feature of maintaining a narrow deposition profile and having the capability to shift the deposition from on-axis to midradius, is extremely effective in shaping the plasma current profile by varying the cofraction and counter fractions. It is also designed to effectively control sawteeth, stabilization and destabilization, and NTMs. Stabilization shall be achieved by driving the co-ECCD just outside the $q = 1$ surface, which helps to flatten the local shear. It may be noted that sawtooth stabilization favors a very narrow and peaked EC current density profile. It also requires an active feedback control system to follow the $q = 1$ surface, which gets displaced due to modification of the local shear by the ECCD. Conversely, the sawtooth period can also be reduced, by driving the current inside the $q = 1$ surface. In this case, neither the deposition width nor its exact location is critical. The sawtooth period can be decreased by a factor of 2 or less with the application of 20 MW of EC power and is achieved from the EL. Besides the above-mentioned roles, another important feature of the EC system at ITER is its role in controlling the NTM instability, which if left unattended, can considerably degrade the fusion burn performance and lead to increased number of plasma disruptions. NTMs, which occur in the outer half of the plasma ($0.6 < \rho < 0.9$), will be controlled by the use of four ULs that have been engineered in such a way as to provide extremely narrow superimposed deposition profiles equivalent to the marginal island width (~4 cm). Note, however, that NTM stabilization lowers the power that can be used for central heating or current drive and hence lowers the Q. At ITER, the NTM control by the EC system will be implemented either by applying the power once an NTM is detected, a slow process taking 2–3 s, or by pre-emptive application of ECCD on a rational q surface to, potentially, avoid the NTM. Another approach could be to toggle the EC power to trigger a sawtooth crash and stabilize the NTM by steering the power from the same steering mirror. The EC system is also used to control the impurities by aiding the pumping out of the tungsten coming from the divertor. A summary plot showing the possible application of the EC system for all the various applications mentioned above is shown in Fig. 1.

III. System Layout and Present Status

The EC system, located on the first (L1) and second (L2) levels of the tokamak building for accessing the equatorial

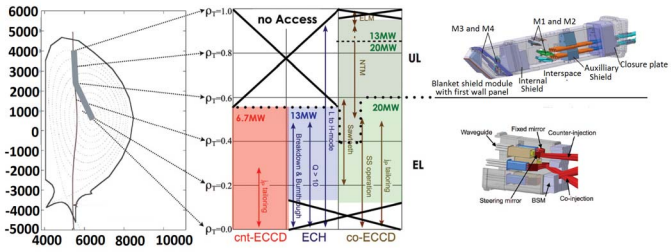

Fig. 1. Summary of EC applications in ITER machine.

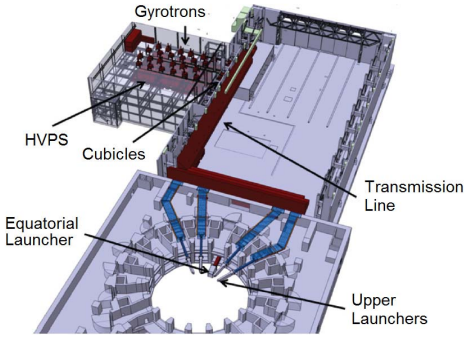

Fig. 2. Layout of EC system at ITER.

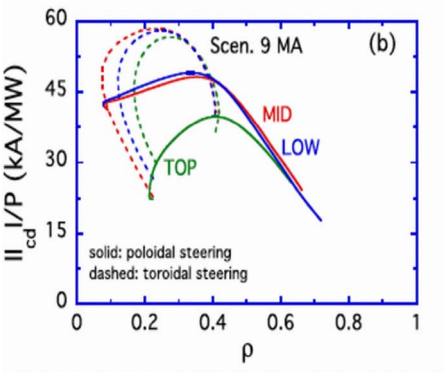

Fig. 3. Driven current for toroidal and poloidal steering.

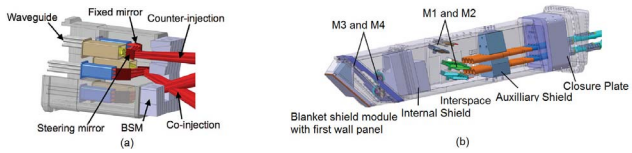

Fig. 4. (a) EL and (b) UL planned for ITER device.

and upper ports, respectively, has a modular design to allow for multiple applications mentioned above at a given time. It is designed to deliver $\geqslant$20 MW at 170 GHz for pulse lengths $\leq$3600 s. The system consists of 24 gyrotrons fed with 12 high-voltage power supplies (HVPSs) located on three levels of the RF building, 24 transmission lines (TL), and five launching antennas. A single main HVPS feeds two gyrotrons, each having its own TL. Each TL, USDA, has an inline switch to enable power being directed to the equatorial launcher (EL) or the upper launcher (UL) with a switching time of 3 s. The 24 TLs from the gyrotrons enter the tokamak building through the assembly hall. The TL switches are located outside the tokamak building wall to allow easy access for maintenance. Inside the tokamak building, the TL passes through the gallery into each port cell. There are secondary confinement barriers at the tokamak wall and port cell penetrations followed by a primary confinement system in the port cell before leading to the launchers in the EL and UL ports. The total power supplied to the EC plant is $\sim$50 MW with an expected delivered power to the plasma of 20 MW. Each of the 24, 1-MW gyrotrons is expected to deliver 0.83 MW to the plasma. The layout of the EC system is shown in Fig. 2.

The design basis for the UL and EL is based on their applications summarized in Fig. 1. UL is required to provide a peaked current density profile with a deposition width of 3–8 cm while accessing the region $0.4 < \rho < 0.8$. The present design of the EL incorporates poloidal steering, which not only provides access out to $\rho \leq 0.6$ but could also double the EC-driven current in the region $0.45 < \rho < 0.6$ as shown in Fig. 3.

The model of the EL poloidal steering system developed by the JADA design team is shown in Fig. 4(a). The design has two slots in the front blanket shield module, instead of the three slots of the earlier design, thus providing improved nuclear shielding. The two slots are shared by three sets of eight beams. The optical design aims at a deposition width of $\sim$30 cm and a transmission efficiency of $\geqslant$96%. The design incorporates three sets of optical mirrors for three horizontal rows, with each set consisting of a fixed mirror followed by a steering mirror, Fig. 4(a). The top row injects beam in the counter direction while the middle and the bottom rows inject beams in the co-ECCD direction.

Each of the four upper launchers, EUDA, Fig. 4(b), has eight entry beams split into two sets of four beams as shown in Fig. 3(b). Each beam is reflected through a four-mirror optical system with the last steering mirror injecting the set of four beams in a vertical plane with $\sim$20° toroidal injection angle to provide the maximum current density for the MHD control. It may be noted that while the upper steering mirrors cover a range of $0.4 \leq \rho_{\text{dep}} \leq 0.88$, the lower ones cover a steering range of $0.6 \leq \rho_{\text{dep}} \leq 0.8$, but both are capable of injecting 3.35 MW. The UL at port 16 is to be used during the first plasma with an injected power level of 6.7 MW for breakdown and burnthrough. The choice of port 16 location minimizes the amount of TL required for installation prior to the first plasma.

A close collaboration between IO, JADA (EL procurement), and EUDA (UL procurement) has resulted in a common configuration for the ex-vessel waveguide, which forms the primary confinement system. The waveguide components are connected using a double helicoflex seal configuration, which allows a double confinement barrier and vacuum monitoring of the interspace. The torus vacuum is separated from the TL vacuum by an isolation valve plus diamond window combination. This allows *in situ* leak testing and window replacement without impacting the torus vacuum. The assembly is located in the port cell outside the bioshield to limit worker radiation

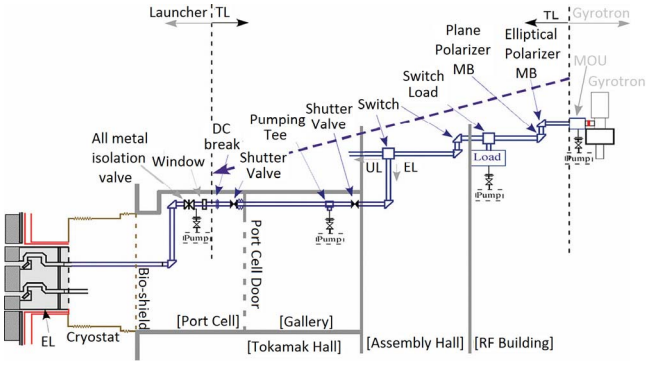

Fig. 5. TL layout for EC system at ITER.

exposure during maintenance. The steering mirrors for the EL and UL also have a common design. The frictionless system, featuring a pneumatic actuator and consisting of the helium pressurized bellows and spring to control mirror rotation, can sweep the steering range in <3 s. Four million full steering cycles with no failure have been achieved. The steering mirrors are expected to undergo ∼60 000 rotation cycles of ∼12°. These cycles correspond to the mirror setting on a shot-to-shot basis.

Each ∼160-m-long TL uses a 63.5-mm HE11 waveguide to transmit the microwaves from the gyrotron to the launchers. Each TL has between 6 and 9 mitre bends (or switches) and includes noncalibrated monitors for forward going power, universal polarizers capable of sweeping the entire range within 2 s with a 98% control on polarization, inline switches, and a switch attached to a load for gyrotron conditioning. The switching action between launchers, which includes shutting off the power applied to gyrotrons, displacing the mechanical switches, and reapplication of the gyrotron voltage, is achieved in <3 s. Fig. 5 shows the layout of a typical transmission line. Over the years, a reduction of space around the port plug has occurred to accommodate degraded assembly tolerances, additional space requirements for plug insertion, and to provide additional neutron shielding in the port region. As a result, the space available at the closure plate is reduced. This requires a reduction in the size of the circular waveguide. As a result, the waveguide inner diameter has reduced to 50 mm as against 63.5 mm for the TL upstream of the diamond window. The change has necessitated a change in the design of the waveguide, coupling, and miter-bends. However, the diamond window diameter is unchanged at 63.5 mm to avoid significant redesign and retesting. The EUDA and Karlschrue Institute of Technology, KIT, have tested the prototype of the window at the Japan atomic energy agency JAEA test facility in Naka using a JADA gyrotron, which was used to transmit 0.82 MW through the window for >100 s. The absorbed power, measured by coolant temperature variation, yielded an estimated loss tangent of 8.4×10^{-6}, well below the required value of 2×10^{-5}. The diamond window is at the JAEA test facility for continued power measurements and longevity studies.

A considerable amount of effort has been put in by USDA in revising the TL component design to minimize higher order modes (HOMs) generated in the waveguide, which would result in higher thermal loads on the connecting sections of waveguides and will generate scattered radiation in the launchers risking overheating of their internal components. The USDA have concentrated their efforts on each of the sources of HOMs and improved the design of the components, which include mitre bend design development to minimize stackup errors during manufacturing and assembly; introduction of inline expansion joints to compensate for thermal variations and building movements; coupling design development to reduce the tilt between waveguides; and R&D to develop straighter waveguides with larger radii of curvatures. Development of a TL Monte Carlo model that allows folding the waveguide component tolerances to estimate the losses is being developed by USDA.

The RF sources for the EC are 24 gyrotrons each operating at 170 GHz and capable of injecting 1 MW for 3600 s into the TLs. The procurement is shared between RFDA (8), JADA (8), EUDA (6) and INDA (2). The development of these sources for the desired specifications has been quite successful. RFDA have tested their third prototype gyrotron achieving 1 MW for 1000 s operation for 97% of the 40 pulses. This achievement has also demonstrated a successful manufacturing process. The EUDA plans to test two prototypes in the 2014–2016 period for the 1 MW gyrotron, which are being developed based on the success of the 140 GHz gyrotrons for the W-7X.

HVPS consists of 12 main, 24 body (BPS), and 8 anode power (APS) supplies. The main PS provides current (∼110 A) and accelerating voltage (∼55 kV) for the gyrotron electron beam. The BPS and the APS provide the additional (∼45 kV) decelerating voltage in a depressed collector configuration, increasing the gyrotrons electrical efficiency to ⩾50%. All HVPSs use the pulse step modulated (PSM) concept to provide the fine voltage control and frequency modulation (≤5 kHz).

The EC system is controlled by an EC plant control consisting of a main plant controller and subsystem local controllers. The architecture of the system is such that it provides the capability of operating the EC system in various modes simultaneously, provide local control, interlock, and hardware information, and communicate with the CODAC and the plasma control system.

IV. IC System

A. Functionality

Many tokamaks operating at the multi-MW level use RF heating. The fast magnetosonic waves experience a large variety of interactions with the plasma particles, including ion cyclotron fundamental and harmonic damping or direct coupling to the electrons' parallel motion. In addition, the fast magnetosonic wave can also be converted into short length electrostatic waves that damp rapidly on the ions or the electrons, depending on the scenario [2].

The energy transfer from the waves to the ions in the ion heating regime causes a tail in the distribution function of the heated species, which can be tailored to some extent by controlling the power deposition profile. This distinct feature

of ICRF assists the L–H-mode transition and/or allows control of burn. In harmonic heating, the wave interacts preferentially with the more energetic ions, a feature that can be exploited to influence energetic particle populations selectively. Further, at resonance condition the presence of the component of the wave vector parallel to the direction of the magnetic induction allows the wave to generate current by launching nontoroidal symmetric spectra, which favors interaction with particles, ions, or electrons, moving toroidally in one or the other direction. In addition, the RF power can be used to create plasma inside the vacuum chamber in the presence of the toroidal magnetic field for wall conditioning, depositing coatings, or for startup assistance. Inducing plasma rotation, though modest compared with that corresponding to the NBs, is another area where ICRF has been successfully applied and tested. The ICRF system therefore provides a flexible tool that can be used for a variety of tasks.

However, the coupling of the RF power becomes difficult if the distance of the antenna is large from the last closed magnetic surface, i.e., the plasma edge. This is due to the fact that in the vacuum region between the antenna and the last closed surface, the electromagnetic field decays exponentially with the distance and the fast wave is evanescent at the antenna. The worst case scenario considered for modeling of the ITER antenna coupling is a combination of a distance of 15 cm from the last closed surface and the short density scrape-off length of 2 cm. These limitations to the coupling will be overcome by a 4-cm outboard shift of the last closed surface. This outboard shift is compliant with the first wall (FW) and the diverter loading [6]. Further, the edge density variations due to edge localized modes (ELMs) cause fast variations in the antenna coupling resistance, which are compensated by the matching scheme to avoid excessive reduction of the average power or generator tripping.

Scenarios relevant to ICRF heating for ITER have been tested in various existing experiments. At high concentrations, minority tails are less energetic and more power is delivered to the background ions leading to $T_i > T_e$. Heavy minority scenarios relevant for the H-phase at ITER have also been investigated. The modeling results indicate good single pass absorption with dominant ion heating for both H-(^{3}He) in ITER at sufficiently low concentrations ($\leq$3%).

The main operating mode of the IC system at ITER is the second harmonic heating of tritium, possibly with a ^{3}He minority. The main asset is the system's capability to couple a dominant fraction of the power to the bulk ions. The system is capable of operation over a wide range of toroidal magnetic fields, 5.3–2.65 T, and the heating scenarios will be available in the pure ^{4}He, H, D, and DT phases. In addition, the system has to provide robust coupling in the presence of ELMs and is designed to perform wall conditioning at low power [$\sim$4 MW] between the plasma shots.

B. System Layout and Present Status

The IC H&CD system at ITER [5] is expected to couple 20 MW of RF power, in the 40–55 MHz range, in a quasi-CW operation with pulse lengths upto 3600 s. The system is spread over four buildings and the two antennas are located in two equatorial ports of the ITER machine. Fig. 6 shows the layout of the ICRF system at ITER. In addition, a test line brings power from the RF source to the port plug test facility located in the hot cell facility.

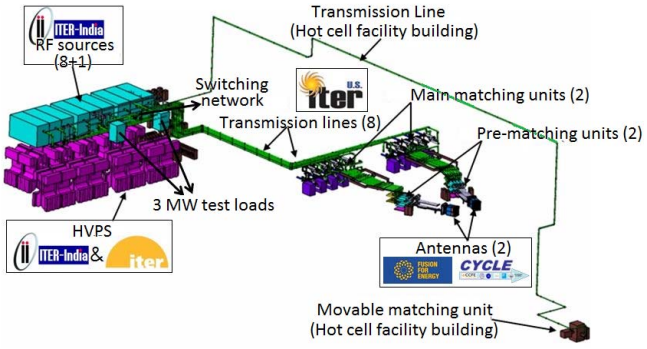

Fig. 6. 3-D view of the ICRF system at ITER.

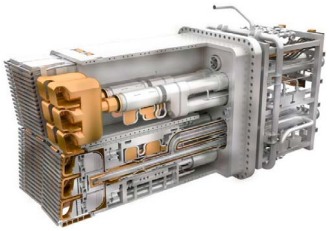

Fig. 7. Cutaway isometric view of the antenna port plug.

Each of the two antennas is designed for a 20-MW capability (capped by the 45 kV limits on the system). The use of two antennas strongly reduces the risks to the system performance associated with uncertainties in the ITER edge density profiles, RF voltage standoff, RF current limit in CW operations, and RF sheath dissipation per antenna. Having two antennas, in addition to being a step in the direction of the future upgrade, not only increases the versatility of the system by allowing for a dual frequency operation but also provides availability during repair operations.

Fig. 7 shows a cutaway isometric view of the IC antenna port plug, EUDA. Each antenna port plug [6] is composed of a support structure, a Faraday shield, the RF structure (antenna radiating box, straps, in vessel vacuum transmission lines, and RF windows), a grounding system, neutron shielding structures, and diagnostics. The 24 radiating straps are arranged in an array comprising of six poloidal and four toroidal straps. The straps are connected so as to form eight poloidal triplets. The control on the toroidal phase differences between antenna voltages or currents and the voltage or current ratios between columns and straps allows control on the radiated power spectrum from these straps. The design and the RF performance assessment is based on the 15-MA inductive H-mode burning plasma scenario. Calculations predict 20–25-MW coupling with two antennas in the baseline second harmonic tritium heating scenario (53 MHz). At the lower end of the frequency range the power would be limited to 10–22 MW in the worst case scenario but above 20 MW

with a plasma outboard shift. Modeling efforts have also revealed the need for adequate RF grounding of the plug to the port extension and also the fact that the voids between the nearby blanket modules and vacuum vessel may influence the RF characteristics. The thermomechanical design accommodates the many requirements and interface constraints to which the plugs are subject. The antenna reference radial position is recessed by 1 cm behind the FW to take care of the sensitivity of the antenna coupling to the distance to the fast wave cutoff. At this location, the antenna is only partially protected from the plasma convective fluxes by the surrounding FW elements. The antenna Faraday shield (FS) is a bar design with each bar consisting of a single channel actively cooled Be-Cu-CuCrZr-SS sandwich. Mockups of such bars with Be layer have been tested successfully upto 3.5 MW/m^2 for 15 000 cycles, well above the expected heat flux of 1.4 MW/m^2. The next qualification step is the manufacturing, high heat flux testing, and the attachment of an FS made of several bars. Further, the four antenna front modules can be radially adjusted by -1 to $+2$ cm around the reference point to achieve the best tradeoff between the plasma convective heat fluxes and RF coupling.

The transmission line USDA is a 300 mm, 50-Ω coaxial transmission line rated for CW transmission of $\sim$6 MW per line with a voltage standing wave ratio (VSWR) $\leq$1.5. The external conductors of these lines will be water cooled and the lines will be filled with dielectric gas at 3 bar to improve the voltage standoff. Circulation of the gas between the inner and outer conductors allows for cooling of the inner conductor.

The matching system, USDA, uses two stub tuners in conjunction with the ELM dump scheme based on 3 dB hybrid power splitters. Such an arrangement provides resistance to variations in the antenna resistive loading, which could be provoked for example by ELMs or transitions from the L–H-confinement mode. Mutual coupling between antenna straps will be overcome by decoupling networks. A prematching system near the antenna performs a first match and lowers the losses between the antenna and the matching system, remotely located in the assembly hall.

The 9 RF sources are rated to deliver either 2.5 MW in CW operation on a VSWR = 2 (36–65 MHz), or 3 MW CW on VSWR = 1.5 in the antenna design band. The sources will use two parallel amplifier chains with a combining circuit. Each amplifier chain consists of a predriver, driver, and final stage. A quarter wavelength combiner is chosen to save space. The ITER specifications of high power coupled to high VSWR and CW operation are challenging and have never been achieved from the high-power tubes available from industrial suppliers. The allocated space for each RF source is 3.6 m $\times$ 9 m $\times$ 5 m.

HVPSs are based on a pulsed step modulator (PSM) design. A large number of low-voltage ($<$1 kV) modules will be stacked in series and can be switched ON/OFF individually for fine regulation of the output voltage. The IC H&CD HVPS system includes a total of 18 identical PSM-based HVPS units. Each unit will supply both the driver and the final stage of one amplifier chain of an RF source. During high-power operation the driver stage is operated at $\sim$14–15 kV while the final stage can be operated to $\sim$27 kV for a maximum output power of 3 MW from two stages. The end stage anode voltage is closed-loop controlled to optimize the tube working point.

A plant system controller will manage the overall operation, safety, and investment protection.

The complete IC H&CD system at ITER is spread over four buildings and two equatorial ports. The RF building houses the power supplies with the transformers, levels 1 and 2, and the ICRF transmitters, 9 RF sources, with the associated transmission lines and dummy loads, level 3. Four RF sources feed one antenna and a switching network allows replacing any of the eight sources by the spare source. The switching network is also used to connect any of the RF sources to the high-power test loads and to a transmission line that allows bringing RF power to the port plug test facility located in the hot cell. The group of eight transmission lines, routed from level 3 to level 2 in the RF building, enters the assembly hall where it connects to the matching system. The matching system assembled on a steel structure and supporting all the RF components is installed on the south wall of the tokamak building and will follow the building movement to ensure minimal stress transmission to the lines in a seismic event. Eight output power lines from each matching system enter the gallery of the tokamak building through a large opening in the 1.5-m thick wall, which is also the safety confinement boundary. As the inner gallery is at a pressure lower than that outside the building, a large metallic sealing flange connected to the transmission lines is used to provide the desired air tightness. The requirements covering shielding, air tightness, and fire resistance for normal and accidental cases are still under discussion. These lines are coupled to the prematching system in the port cell where each of the eight circuits consists of three stubs to cover the range of loads and frequencies. The prematching network in the port cell then connects to the antenna through a complicated network of transmission lines passing through the bioshield plug. The lines include axial and radial flexible components to decouple the relative movement of the antenna attached to the tokamak flange from the prematching system. Achieving the density of the equipment and the access for installation and maintenance is a challenge. Most of the components need to be removed to access the antenna. The antennas are located on the equatorial ports and the gap between the antenna and the port extension is a compromise between the need to reduce the neutron streaming and the clearance for assembly operations. The present neutronic modeling indicates a shutdown dose rate in excess of the initial target. The present antenna design includes custom-machined shielding plates to reduce the gap between the port extension and the antenna to 9 mm over the 80 cm length near the back flange. The final vacuum sealing design options of lip welds or double seal vacuum gaskets is under study. The progress of the antenna design awaits finalization of the installation scheme and sealing options.

The responsibility of the procurement of different components of the complete ICRH system involves EUDA, INDA,

Fig. 8. Resonant ring for transmission line component testing in ORNL, USA.

and USDA. The antenna manufacturing and testing activities are being managed with the EUDA. The prototype activities include manufacturing and testing of FS bars with the Be layer and also the FS prototype with several bars. The key outstanding issues are the validation of the nuclear shielding solution for the gap between the port plugs and the tokamak port extension, without putting RF performance at risk, design of the FS bar attachment, remote handling replacement of FS modules during maintenance, validity of high current radio frequency (RF) contacts underway at a test facility in IRFM Cadarache, and qualification process of the brazed alumina RF windows. It may be noted that the RF window qualification is to be documented as a part of the tritium boundary and the safety qualification roadmap includes material qualification and prototyping. For the transmission line and matching components, a complete qualification program is underway at the USDA where an RF resonant ring (see Fig. 8) is used to test the components at the ITER specification level; components have been tested with circulating power levels in the range of 6 MW for a 1-h duration. The required R&D for the development and availability of the RF power sources is being coordinated by the INDA, who have placed two R&D contracts with Thales electron devices and Continental Electronics for two known power tubes, CPI 4CM2500KG tetrode, and TED TH628 diacrode. Factory tests in excess of 1.5 MW for several thousands of seconds have been performed recently over the desired ITER frequency range and the final choice of the supplier for ITER sources is foreseen next year. Final tests with tubes and cavities integrated in a full amplifier chain developed by the INDA will be performed at the INDA test bed to validate the complete design as per ITER specification. As a result, besides tube qualification integration work related to component layout is also underway at the INDA to ensure that all the components including amplifier chains, combiner, local control unit, water cooling pipes, and power supply cables fit within the allocated space restriction. As far as the HVPSs are concerned, the design of a prototype unit, consisting of 48 PSM modules, each with a rated voltage of 740 V has been performed by the INDA and was reviewed to validate the design choices. Specifications of the individual components have been finalized. The components based on their dimensions have been integrated in a CAD model to ensure building space allocation and define the interface points. The modules and the filter inductor are integrated in a metallic cabinet to minimize electromagnetic interference and ensure occupational safety.

V. NB H& CD

NB [7] in tokamak machines worldwide have proved to be efficient not only in producing high plasma temperatures but also in driving plasma current and to produce plasma rotation. The basic processes that lead to beam trapping and the subsequent coupling of energy and momentum to the plasma are well understood and are in good agreement with the theoretical predictions. The coupling efficiency is insensitive to the initial shape and configuration of the plasma and its isotopic composition. It is also unaffected by any changes that may result from heating the plasma, e.g., ELM and sawtooth behavior, transitions to different modes of confinement, and subsequent changes to the plasma profile. In order to penetrate to the center of the large ITER, plasma beam energies in the range of 250–500 keV/amu are required.

The spatial dependence of power deposition by the injected NBs is determined mainly by the ionization cross sections of the NB and the plasma electron density profile. NBs suffer multistep ionization, i.e., excitation and subsequent ionization of the excited neutral atoms, and this must be taken into account in determining the deposition profile. Post ionization, the fast ions produced in the plasma slow down by coulomb interaction with the plasma electrons and ions thereby heating the plasma. Reduction in the heating efficiency can occur because of losses of fast ions via toroidal magnetic field ripple and interaction with the MHD and other instabilities. Further, fast particle losses also result from the toroidal Alfven eigenmode (TAE) resonances, which will be avoided at ITER by the choice of an appropriate injection angle for a fixed beam energy. Another important feature to consider is the beam shine through, which is dependent on the electron temperatures and the plasma density. Estimations indicate that for almost all the scenarios for ITER, the shine through is $\sim$1% which is small in terms of NB performance but which requires a careful evaluation of the design of the FW due to potentially high power densities on the wall, particularly at low plasma densities.

Another area where the NBs have been used effectively is the current drive, i.e., producing current parallel to the magnetic axis in addition to the conventional inductive drive. In the case of NBs, it is the parallel velocity component of the suprathermal ions created from the injected neutrals that is responsible for driving a toroidal current. The current drive efficiency is defined as the ratio of the driven current to the injected NB power and is mainly determined by the basic characteristics of the fast ion thermalization process. The process is however strongly influenced by the presence of ions and electrons in the trapped banana orbits in tokamak plasmas of low collisionality. The NB-driven current density has a radial profile that depends on the beam energy, the deposition profile, and the injection angle. It is possible to optimize these aspects to some extent in order to achieve the desired NB-driven current profile shape and to maximize the global current drive efficiency related to the injected power. The highest efficiency is achieved at the highest electron temperature and the lowest density in the tokamak, and by choosing the beam energy close to the critical energy at which the effects of collisions with the thermal ions and

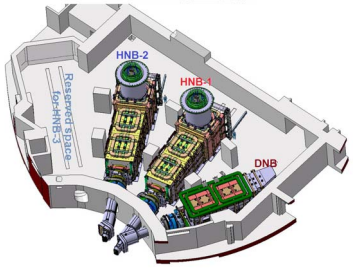

Fig. 9. HNB-1 and HNB-2 layouts at ITER. Also shown is the reserved space for the third HNB for future upgrade.

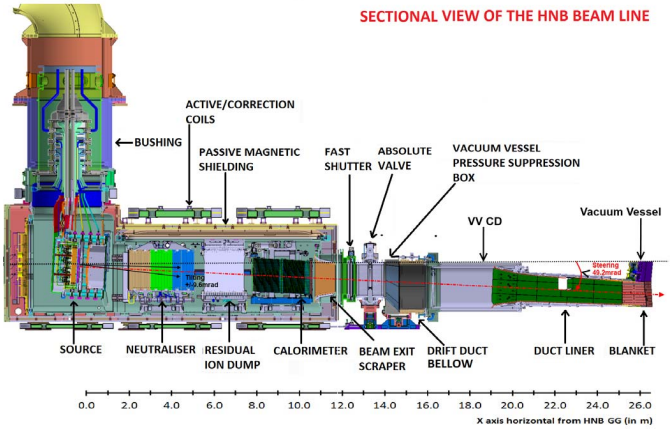

Fig. 10. Cutaway view of the HNB injector at ITER.

electrons are approximately equal. In practice, however, the choice of beam energy is determined by the beam penetration requirements.

NBs inject momentum into the plasma, hence, they can induce plasma rotation when not injected normal to the plasma axis. Of all the auxiliary heating schemes, NB is the one that imparts the highest toroidal momentum to the plasma. Plasma rotation in ITER produced by the NBs has been computed for various beam energies and target plasma densities. The results show that while the central angular velocity is insensitive to the beam energy, the velocity at the outer surface is quite strongly dependent on the beam energy due to a reduced penetration and a high specific momentum input per unit power input.

At ITER, two heating NB (HNB) lines shall be installed in the NB cell and connected to two equatorial ports of the machine. The HNB-1 beamline has a crossover in the duct region with the neighboring DNB beamline. An additional equatorial port is reserved for an upgrade of the additional heating by the installation of the third HNB. Fig. 9 shows the layout of the two beamlines with a possible upgrade to the third beamline if required. The beamlines will be operated during the H-He, DD, and DT phases of ITER operation. Each HNB beamline consists of a vacuum vessel housing an eight-driver RF-based negative ion source with an extraction area of 1.53 m in height and 0.58 m in width coupled to a seven-grid ion extractor and accelerator system, a four-channel neutralizer followed by a four-channel residual ion dump, and a beamline calorimeter. The two panels of the calorimeter can be opened or closed in vacuum. In the open position, the beam passes between the two panels to the tokamak, and in the closed position the panels form a V shape, which intercepts the beam. The calorimeter allows commissioning of the injector independent of ITER, and it will be used as a diagnostic tool to characterize the beam before its injection into the machine. The various hydraulic, high voltage, and RF feed lines to the source and the extractor and accelerator system are connected from their points of origin to their corresponding ends in the source through a high-voltage bushing placed at the top of the vessel. The walls of the vacuum vessel are lined with cryopumps to reduce the gas density between the beam source and the neutralizer and downstream of the neutralizer in order to minimize the losses in the accelerator and reionization losses downstream of the neutralizer. The layout of components is shown in Fig. 10.

The vacuum vessel exit is connected to the ITER machine port through a series of front end components consisting of a fast shutter, a drift duct bellow, an absolute valve, a vacuum vessel pressure suppression system box, a connecting duct with a liner, and a ∼6-m-long duct. The total distance from the grounded grid of the accelerator to the entrance into the tokamak is ∼26 m. The desired beam parameters and the injection angles to obtain off-axis current drive and to avoid beam-excited TAE in the ITER plasma are listed in Table II. It may be noted that ∼40 MW of power is required to be launched from the ion source in order to meet the goal of 16.5 MW per beamline injected into ITER. The remaining power is lost as unneutralized ions coming out of the neutralizer (∼40%), which are deposited on the walls of the residual ion dump, and beam transport losses because of the finite divergence of the beamlets, the existence of a high divergence beam halo and the inaccuracies in the beam alignment leading to a direct interception of the beam with the various surfaces of the components mentioned above, and reionization loss from the NB due to collisions with the residual gas between the entrance of the RID and the tokamak.

The beams at ITER are expected to be operated over a wide range of plasma scenarios. These include those corresponding to the full and half plasma currents of 15 and 7.5 MA, respectively. In addition, NB injection for the 5-MA plasma current scenario is also considered if the plasma density in the ITER machine is sufficient to avoid beam shine through damaging the FW of the machine. The production of the beams requires considerable modeling efforts related to the optimal physics design of the accelerator, which defines the beam optics for beams and includes considerations like beamlet divergence, suppression of coextracted and stripped electrons in the accelerator, and their corresponding loads on the grids, beamlet steering by the extractor grid, EG and the grounded grid, GG lenses and its compensation, compensation of beamlet deflection due to space charge repulsion between the beamlets, the power corresponding to the electrons leaking out of the accelerator, and the horizontal and vertical focusing of the beamlets and the beam groups. The transport of the

TABLE II
ITER NEUTRAL BEAM PARAMETERS

Parameter		HNB
Injected neutral beam power (HH/HHe, DD/DT phase) (MW)		16.5 per beamline
Beam energy / species (HH/HHe Phase)	(MeV)	0.87 / H
Beam energy / species (DD/DT Phase)	(MeV)	1 / D
Accelerated current (HH/HHe Phase)	(A)	46 / H
Accelerated current (DD/DT Phase)	(A)	40 / D
Beamlet divergences (HH/HHe, DD/DT Phases)	(mrad)	3, 5, 7*
Halo component (HH/HHe, DD/DT Phases)	(%/mrad)	15/30
Pulse length/Duty cycle	(s)	3600/25%
Total time of beam operation	(s)	2 x 10^7
Horizontal focussing beamlet/beam group	(m)	7.2 / 25.5**
Vertical focussing beamlet/beam group	(m)	Infinity/25.5**
NBI axis vertical inclination angle	(mrad)	-49.2
Beam axis vertical tilting angle	(mrad)	+/- 9

*Values assumed for the design of the injectors.
**Groups of beamlets from the accelerator are aimed to co-incide at 7.2 m in the horizontal direction, but they are all nominally parallel in the vertical direction. The beams from each of the 4 vertically stacked segments of each grid of the accelerator are inclined so that the beams co-incide at 25.5 m.

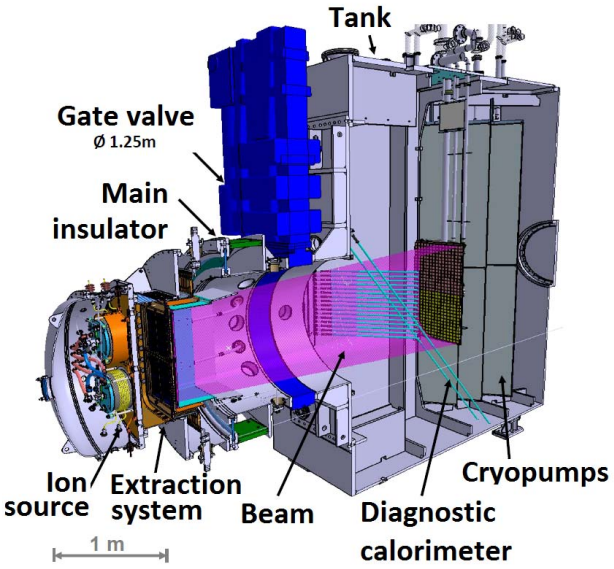

Fig. 11. Cutaway view of ELISE facility at IPP.

beams from the grounded grid of the source to the plasma also requires careful design efforts to ensure the maximum transmission with a minimal loss of the beam due to a direct interception with the surfaces that the beam comes in contact with during the transport and to take into account the power loads due to the reionized ions that get deflected because of the magnetic fields from the tokamak, depending on the scenario of operation. Based on the physics inputs related to these studies, the thermomechanical design of the beamline and front end components and the duct liner have been carried out to ensure that they survive the full life cycle of ITER, i.e., 20 years.

Neutrons from the fusing ITER plasma can flow through the NB openings in the tokamak wall and through the NB duct and into the injectors. The passive magnetic shields (PMSs) surrounding each injector consist of a double layer of steel with a total thickness of 150 mm. Detailed nuclear analyses have been carried out to determine the shutdown dose rates in the NB cell and radiation levels outside the NB cell. Filling the interspace of the PMS with 100-mm-thick polyethylene and cladding the external PMS surfaces with 10–25-mm-thick lead reduces the shutdown dose rate to acceptable levels of <100 μSv/h in all areas where human access is required.

The success of NBs at ITER depends on the successful prototyping of a large number of components, as this is the first time that components of this size with novel concepts are planned to be used. The first in the series is the eight-driver RF-based negative ion source. In the past, H & D beams with ITER desired current densities and with the desired electron-to-ion ratio for pulse lengths upto 3600 s have been demonstrated on the single driver RF sources at IPP [8]. However, it is important to establish similar or even better behavior for ITER-sized sources The 1280 beamlet, seven-grid extractor and the accelerator system consists of five accelerating gaps of 200 kV each, in order to reach a beam energy of 1 MeV. It is not only large in size but also has novel concepts related to compensation of the beamlet deflection by the electron suppressor magnets embedded in the extraction grid, the use of segments with angled beam groups for horizontal aiming and inclination of the segments for vertical aiming of the beams from the segments, the use of kerbs [9] between the beam groups for focusing the beamlets horizontally at the exit of the channel of RID, and the suppression of stripped electrons by magnets in the accelerator grid along with the long-range filter field to reduce the electron leakage from the accelerator. The manufacturability and assembly of this accelerator system not only needs to be established but its performance also needs to be validated through experiments. Another area that requires validation is the successful functioning of the electrostatic residual ion dump (RID), which deflects the positive and negative ions from the beam. The deflected ions are dumped on the channel walls of RID. On the component level, several of the components like the large diameter ceramic rings for the 1 MV bushing, post insulators, the safety important class SIC feedthroughs, dissimilar metal joints, etc., also need extensive prototyping to validate their design and manufacturing as per the ITER requirements of materials, manufacturing techniques, and safety requirements. These issues are under assessment and at various stages of execution. In order to validate the source design and to establish the operational parameter space of the RF negative ion sources, a four-driver-based RF negative ion source facility, ELISE [10], (Fig. 11) is operational at IPP.

Experiments are underway at the facility with both H-beams and D-beams, and the up-to-date achievements are listed in Table III.

While the ITER parameters for operation with H-beams are almost established, the development for operation with D-beams is continuing. The obtained electron-to-ion ratio with D-beams is higher than the ITER requirement and unstable during long pulses. Further experiments are planned this year to establish the desired parameter space

TABLE III

PRESENT ELISE STATUS COMPARED TO ITER BEAM REQUIREMENTS

Parameter	H^- beam	D^- beam	ITER*
Gas filling pressure (Pa)	0.3	0.3	≤0.3
Beam current accelerated (A)	20	15	20 (23)
Extracted current density (mA/cm2)	26	20	29 (33)
RF power for max current density (kW)	2 x 110	2 x 110	≤2 x 200
Max pulse length for high power pulses (s)	10	3	3600 (1000)
Max pulse length for lower power pulses (s)	450 (3600)	10	3600 (1000)
Electron to ion ratio	0.4	1.06	<1, (0.5)
Current density scaling with power	Linear	Linear	

*Numbers in parentheses refer to H operation.

Fig. 12. PRIMA test facility at RFX, Padua, Italy.

of ITER requirements in terms of beam production and characterization for H and D beams at full RF power and long pulse lengths.

In addition to this a complete source and beamline component testing facility, PRIMA [11] (see Fig. 12) is being established at RFX, Padua, Italy. The PRIMA buildings are nearing completion. The facility consists of two testbeds named SPIDER [12] and MITICA [13]. The SPIDER facility will test the full-sized ITER source to establish its performance for both H-beams and D-beams for energies upto 100 keV. The facility consists of a vacuum vessel housing the source, several diagnostics that include Langmuir probes, thermocouples, various kinds of optical diagnostics, a carbon tile-based calorimeter to view the individual beamlets and to characterize the beam, and an INDA-contributed ion dump instrumented with thermocouples. The SPIDER source is under manufacture. It is managed by EUDA. A consortium of companies including Thales, France, CECOM, Italy, and Galvano T, Germany are responsible for the manufacturing the various parts and delivery of the assembled source. The vacuum vessel, manufactured by ZANON, has been delivered to the RFX site. Installation and acceptance tests are underway. The source manufacturing was completed by the end of 2015. The assembly of source at the factory site is underway and the source is expected to be delivered to the Padua site in the second half of 2016 followed by source integration and operation. The ion source and extraction power supplies for SPIDER are being procured by the EUDA, and the 100-kV acceleration power supply is being procured by the INDA.

The MITICA facility will house a full ITER-sized beam source capable of accelerating 40 A D^- beams to 1 MV (0.87 MV and 46 A with H^-) and the beamline components, i.e., the neutralizer, RID, and the calorimeter are identical to those designed for the ITER HNBs. For the MITICA source, all experiences from the SPIDER source manufacturing will be folded in. The source components will be manufactured as far as possible according to the required ITER standards to gain experience and establish technologies for the actual HNB components. The final design review for the MITICA beam source and the beamline components (BLCs) has been completed and the technical specifications leading to the call for tender are under preparation. Full-scale prototypes for some of the components like the post insulators, swirl tubes, etc., have been initiated by RFX. The procurement of the vessel and the various PS systems are either already assigned or under call for tender. By the end of 2015, all the tenders were launched and most of the procurements were assigned. All JADA supplies [14] are currently under manufacturing by Japanese firms. The installation phase of the TL and HV PS components which started in December 2015 will continue until spring 2017. This phase will be followed by the integrated commissioning of all plant and interlocks with CODAS and by the PS integrated tests. The MITICA BS will be installed in 2019 and will be followed by an experimental phase dedicated ion source and BLC to achieve the ITER parameters. More details of the present status of the NB system can be found in [15].

VI. CONCLUSION

The physics requirements and the progress underway to achieve the three auxiliary systems, the EC, IC, and NB have been described in this paper.

ACKNOWLEDGMENT

The authors would like to thank the contributions from all the scientists and engineers of the participating DAs, whose names could not be listed here, but whose contributions were recognized for their immense role in reaching the present stage of this work. The views and opinions expressed herein do not necessarily reflect those of the ITER Organization.

REFERENCES

[1] M. Shimada *et al.*, "Chapter 1: Overview and summary," *Nucl. Fusion*, vol. 47, no. 6, pp. S1–S17, Jun. 2007.

[2] ITER Physics Expert Group on Energetic Particles, Heating and Current Drive and ITER Physics Basis Editors, "Chapter 6: Plasma auxiliary heating and current drive," *Nucl. Fusion*, vol. 39, no. 12, pp. 2495–2539, Dec. 1999.

[3] F. Wagner *et al.*, "On the heating mix of ITER," *Plasma Phys. Controlled Fusion*, vol. 52, no. 12, p. 124044, Nov. 2010.

[4] M. Henderson *et al.*, "The targeted heating and current drive applications for the ITER electron cyclotron system," *Phys. Plasmas*, vol. 22, pp. 021808-1–021808-15, Feb. 2015.

[5] P. Lamalle *et al.*, "Status of the ITER ion cyclotron heating and current drive system," in *Proc. AIP Conf.*, vol. 1689. 2015, p. 030007.

[6] P. Lamalle *et al.*, "Status of the ITER ion cyclotron H&CD system," *Fusion Eng. Des.*, vol. 88, nos. 6–8, pp. 517–520, Oct. 2013.

[7] R. Hemsworth *et al.*, "Status of the ITER heating neutral beam system," *Nucl. Fusion*, vol. 49, no. 4, pp. 045006–045020, Mar. 2009.

[8] P. Franzen *et al.*, "Progress of the development of the IPP RF negative ion source for the ITER neutral beam system," *Nucl. Fusion*, vol. 47, no. 4, pp. 264–270, Mar. 2007.

[9] H. P. L. de Esch *et.al.*, "Physics design of the HNB accelerator for ITER," *Nucl. Fusion*, vol. 55, p. 096001, 2015.

[10] B. Heinemann *et al.*, "Negative ion test facility ELISE—Status and first results," *Fusion Eng. Des.*, vol. 88, pp. 512–516, 2013.

[11] V. Toigo *et al.*, "Progress in the realization of the PRIMA neutral beam test facility," *Nucl. Fusion*, vol. 55, no. 8, p. 083025, 2015.

[12] D. Marcuzzi *et al.*, "Detail design of the beam source for the SPIDER experiment," *Fusion Eng. Des.*, vol. 85, nos. 10–12, pp. 1792–1797, Dec. 2010.

[13] P. Agostinetti *et al.*, "Detailed design optimization of the MITICA negative ion accelerator in view of the ITER NBI," vol. 56, no. 1, p. 016015, 2015.

[14] K. Watanabe *et al.*, "Design of a–1 MV dc UHV power supply for ITER NBI," *Nucl. Fusion*, vol. 49, no. 5, pp. 055022-1–055022-5, Apr. 2009.

[15] M. J. Singh *et al.*, "Heating neutral beams for ITER; present status," in *Proc. SOFE*, Austin, TX, USA, 2015.